The Structure of the Proton

Robert Lahmann
on behalf of the H1 and ZEUS collaborations
DESY-H1
Notkestr. 85
22607 Hamburg
e-mail: lahmann@@mail.desy.de

Abstract

Recent results from the HERA experiments H1 and ZEUS are presented with respect to their contribution to the understanding of the inner structure of the proton. With the large 1997 statistics, the proton structure function F_2 has been measured with remarkable precision over a wide kinematic range. At low Q^2, in the transition region between deep inelastic scattering and photoproduction, new measurements explore a previously unprobed kinematic region and allow comparisons with different theoretical models. Furthermore, new results of the longitudinal proton structure function F_L and the charm contribution F_2^c to F_2 are discussed. Finally, measurements of the gluon distribution from scaling violations of F_2, charm production and dijet events are presented and compared. All results are consistently described within the framework of perturbative QCD.

1 Introduction

The precise measurement of the inclusive neutral current deep inelastic ep scattering (DIS) cross section $\sigma(ep \to eX)$ with the H1 and ZEUS detectors at HERA is essential for investigating the proton structure and for precision tests of QCD. Both detectors have been operating since 1992 and in 1997, HERA delivered an annual luminosity of about 35 pb^{-1} which more than doubled the combined luminosity from the previous years.

Up to 1997, with electron[1] and proton beam energies of $E_e = 27.5$ GeV and $E_p = 820$ GeV, respectively, HERA was operating at a center of mass energy of $\sqrt{s} \equiv \sqrt{4E_eE_p} \approx 300$ GeV.[2]

With this center of mass energy, the accessible kinematic region was extended by more than two orders of magnitude in the Bjorken scaling variable x and the squared four-momentum transfer Q^2 compared to previously available data from fixed target experiments. At values of Q^2 much less than the squared mass of the Z^0 ($Q^2 \ll M_Z^2$), DIS interactions are dominated by the exchange of photons. In this kinematic region, the double differential DIS cross section $d^2\sigma^{ep}/(dxdQ^2)$ is parametrized by the structure functions F_2 and F_L. Introducing the reduced cross section σ_r, one defines

$$\sigma_r \equiv \frac{d^2\sigma^{ep}}{dxdQ^2} \cdot \frac{Q^4 x}{2\pi\alpha^2 Y_+} = F_2(x,Q^2) - \frac{y^2}{Y_+} F_L(x,Q^2) \ , \tag{1}$$

where $Y_+ = 1 + (1-y)^2$ and the inelasticity is defined as $y = Q^2/(xs)$. Effects due to the coupling of the Z^0 have to be taken into account for values $Q^2 \gtrsim 5000$ GeV^2; this kinematic regime is treated in a separate paper [1] and will not be discussed here.

In the quark parton model (QPM), the structure functions are given by $F_2(x) = x\sum_{i=1}^{n_f} e_i^2[q_i(x) + \overline{q}_i(x)]$ and $F_L = 0$ for spin $\frac{1}{2}$ partons. As will be described below, in perturbative QCD (pQCD) the parton distributions also have a Q^2 dependence and F_L is not identical zero.

As Q^2 becomes small, α_s becomes large and pQCD finally breaks down. As will be discussed in this paper, cross section measurements have been performed by H1 and ZEUS in the region $Q^2 \lesssim 1$GeV^2, thereby probing the transition region between photoproduction and DIS. Furthermore, measurements of the charm contribution to the proton structure function F_2^c and various methods to extract the gluon distribution from the data recorded by H1 and ZEUS will be discussed.

[1] HERA operated with positrons between 1994 and 1997. The expression 'electron' will be used throughout this paper to refer to both electrons and positrons.

[2] Data from 1998 onwards, when HERA increased the proton energy to $E_p = 920$ GeV, will not be presented here.

2 QCD Analysis

In perturbative QCD, the Q^2 evolution of the parton distributions is described by the DGLAP [2] equations. Using the flavor singlet and nonsinglet quark distributions $x\Sigma(x) = x\sum_{i=1}^{n_f}(q_i(x) + \bar{q}_i(x))$ and $xq^{NS}(x) = x\sum_{i=1}^{n_f}(q_i(x) - \bar{q}_i(x))$, of which $q^{NS}(x)$ evolves independently of the gluon, the equations can be formulated as follows:

$$
\begin{aligned}
\frac{\partial}{\partial \log Q^2} \; q^{NS}(x,Q^2) &= \frac{\alpha_s}{2\pi} \; P_{qq}^{NS}(x/\xi) \otimes q^{NS}(\xi,Q^2) \\
\frac{\partial}{\partial \log Q^2} \begin{pmatrix} \Sigma(x,Q^2) \\ g(x,Q^2) \end{pmatrix} &= \frac{\alpha_s}{2\pi} \begin{pmatrix} P_{qq}(x/\xi) & P_{qg}(x/\xi) \\ P_{gq}(x/\xi) & P_{gg}(x/\xi) \end{pmatrix} \otimes \begin{pmatrix} \Sigma(\xi,Q^2) \\ g(\xi,Q^2) \end{pmatrix} .
\end{aligned} \tag{2}
$$

Here $\otimes$ denotes the convolution integral $P \otimes p \equiv \int_x^1 \frac{d\xi}{\xi} P(x/\xi) \cdot p(\xi)$. and the splitting functions P_{ij} represent the probabilities for a parton j with momentum ξ to radiate a parton i with momentum $x < \xi$. For the parton distributions xq and xg a parametrization in x is chosen which is fitted to the data at a starting value Q_0^2 and the DGLAP equations (2) are used to evolve the parton distributions to any Q^2.

The H1 and ZEUS collaborations use slightly different parametrizations for their fits. Details on the parametrization and the experimental procedure can be found elsewhere [3], [4]. The functional form of the parametrization chosen by both collaborations is

$$xp(x) = A_p x^{B_p}(1-x)^{C_p}(1 + D_p x + E_p\sqrt{x}) \; , \tag{3}$$

where $p = g, u_v, d_v, S$ in the case of H1 and $p = g, \Delta_{ud}, S$ in the case of ZEUS. The valence quark distributions of the u and d quarks are defined as $xu_v \equiv x(u - \bar{u})$ and $xd_v \equiv x(d - \bar{d})$, while $x\Delta_{ud} \equiv x(u_v - d_v)$ denotes their difference. ZEUS takes the input valence quark distributions xu_v and xu_d at Q_0^2 from the parton distribution set MRS(R2) [5]. The sea quark distribution is defined as $xS = 2x(\bar{u}+\bar{d}+\bar{s})$, where H1 assumes $\frac{1}{5}S = \bar{u} = \bar{d} = 2\bar{s}$ while ZEUS assumes $\frac{1}{5}S = 2\bar{s}$ at the scale $Q^2 = 1$ GeV^2 in accordance with MRS(R2).

F_2 is formed from the gluon distribution and the distributions of the three light quark flavors (u, d, s) while the charm contribution is calculated from the photon gluon fusion process including NLO corrections [6]. The contribution of the b quark was neglected. Finally, some of the parameters in equation (3) are fixed by sum rules.

The starting point of the evolution was chosen at $Q_0^2 = 2$ GeV^2 by the H1 collaboration and data with $Q^2 \geq 2$ GeV^2 were included in the fits. The ZEUS collaboration used a starting scale of $Q_0^2 = 7$ GeV^2 and data with $Q^2 \geq 1$ GeV^2 for the fit which implies a forward and backward evolution. Both H1 and Zeus use NMC [7] and BCDMS [8] data obtained for proton and deuteron targets to constrain the high x region.

3 Measurement of F_2

The key components of the ZEUS detector for the F_2 analysis are the Uranium Scintillator Calorimeter (UCAL) and the Central Tracking Detector (CTD). The data used for the 1996-1997 F_2 analysis correspond to an integrated luminosity of 6.8 pb^{-1} in the low Q^2 region and 27.4 pb^{-1} in the high Q^2 region. ZEUS defines the region $Q^2 \leq 22$ GeV^2 as the low and $Q^2 \geq 27$ GeV^2 as the high Q^2 region [9]. The newly installed Beam Pipe Calorimeter (BPC) and Beam Pipe Tracker (BPT), which allow measurements with Q^2 values as low as $Q^2 = 0.045$ GeV^2, will be discussed in section 5.

For the H1 detector, the separation of the high and low Q^2 region is given by the detector instrumentation. Depending on whether the electron is scattered into the central region, which is instrumented with a Liquid Argon Calorimeter (LAr) or into the backward region[3] equipped with a lead-fiber calorimeter (SPACAL), the events are said to have high or low Q^2, respectively. Tracking is done with the central tracker and with a planar Backward Drift Chamber (BDC) in the respective regions. The bins in the low Q^2 region range from 2 GeV^2 to 120 GeV^2 where for $Q^2 < 20$ GeV^2 the newly installed Backward

[3] The HERA experiments have an asymmetric design in order to account for the boost of the ep interactions into the proton direction. The terms forward/backward are used to describe the region near the beam pipe in the proton/electron direction.

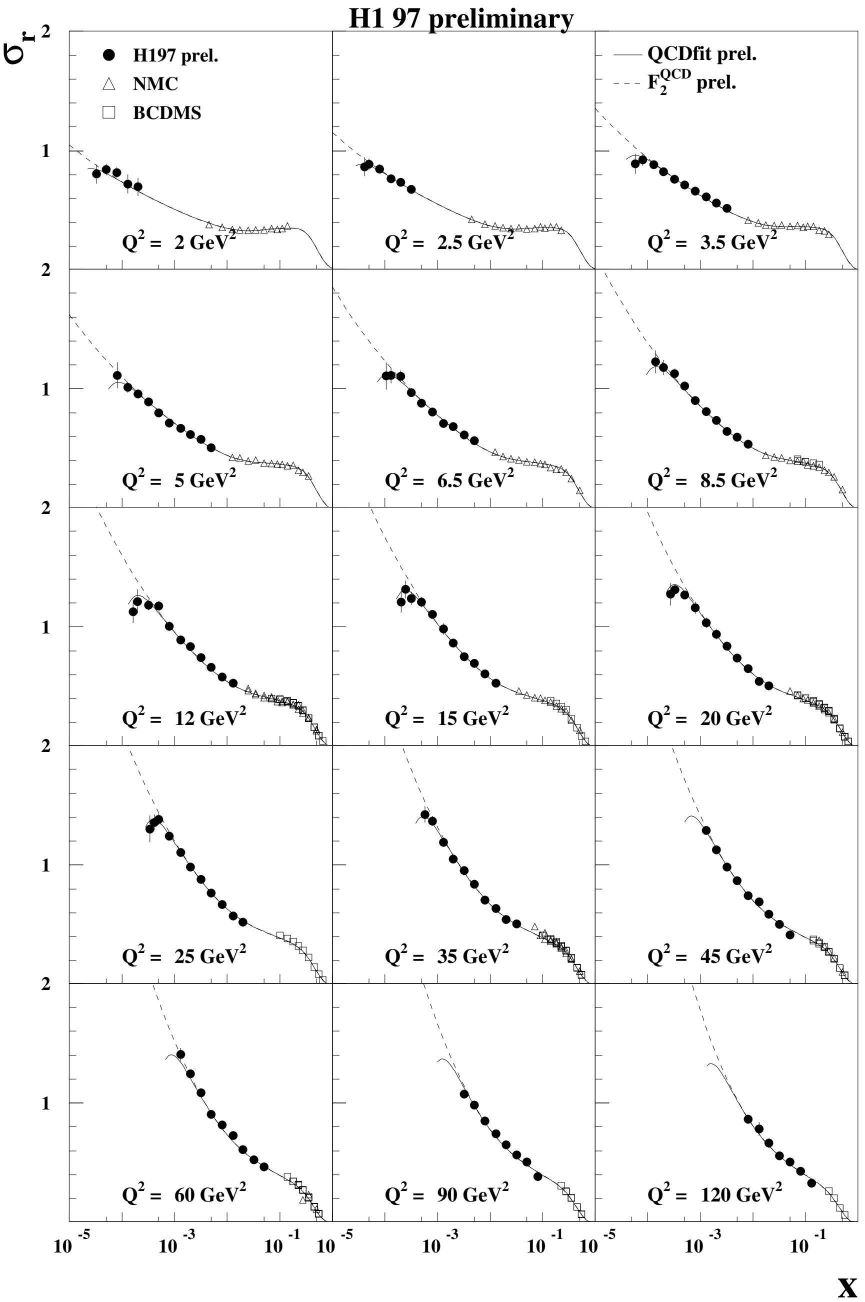

Figure 1: H1 measurement of the reduced cross section as a function of x for Q^2 bins ranging from 2 GeV^2 to 120 GeV^2 (full circles). Also shown are the results from the NMC (open triangles) and BCDMS (open squares) collaborations in the high x region. The solid line corresponds to a NLO QCD fit to the H1, NMC, and BCDMS data, the dashed curve denotes the structure function F_2 determined with this fit.

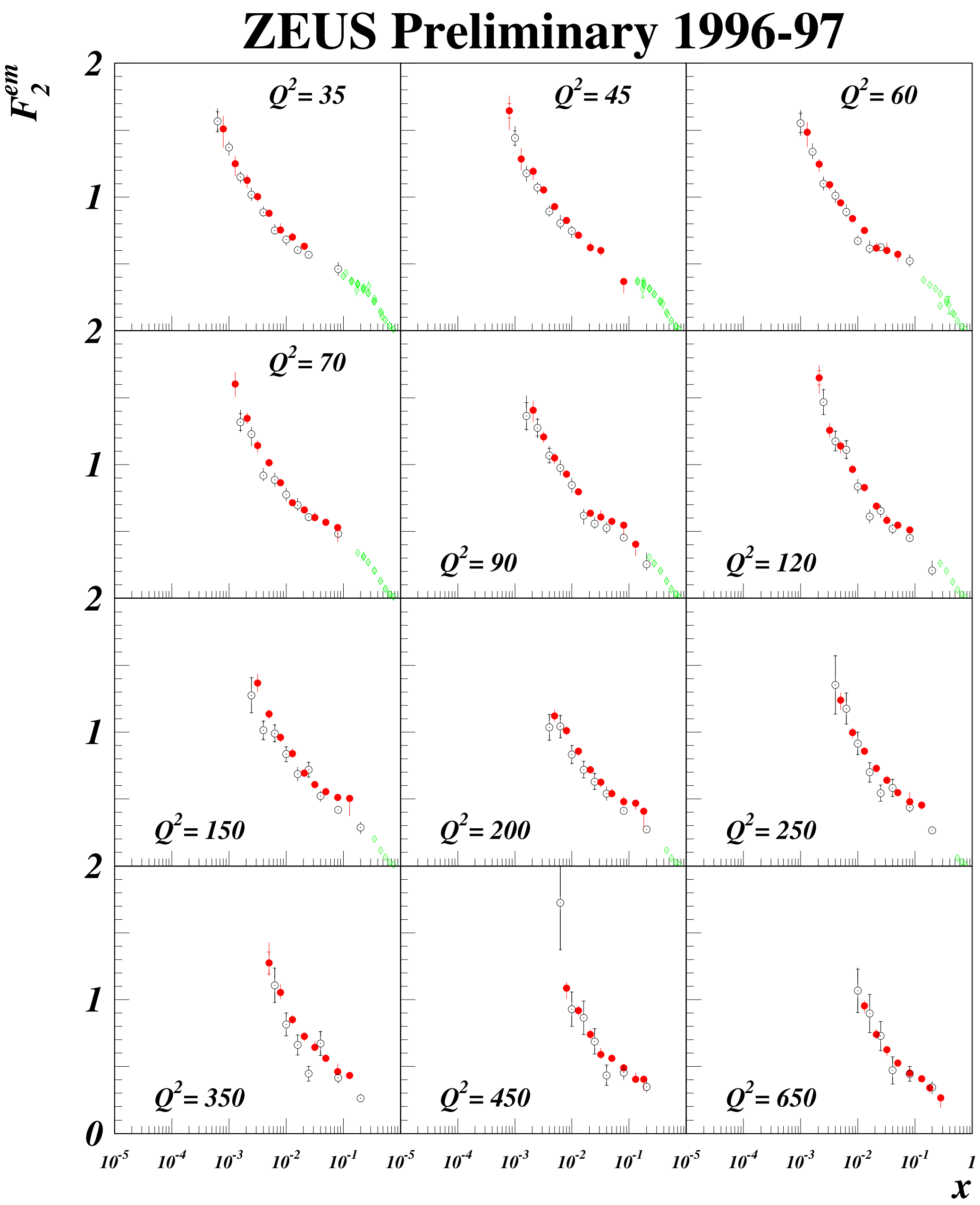

Figure 2: ZEUS measurement of F_2 in the medium Q^2 region. The full circles and dashed bars correspond to the measurement described in the text, the open circles and solid bars show the 1994 ZEUS results. The inner error bars show the statistical errors, the outer error bars the statistical and systematic errors in quadrature. The diamonds correspond to the fixed target results in the high x region from BCDMS and NMC.

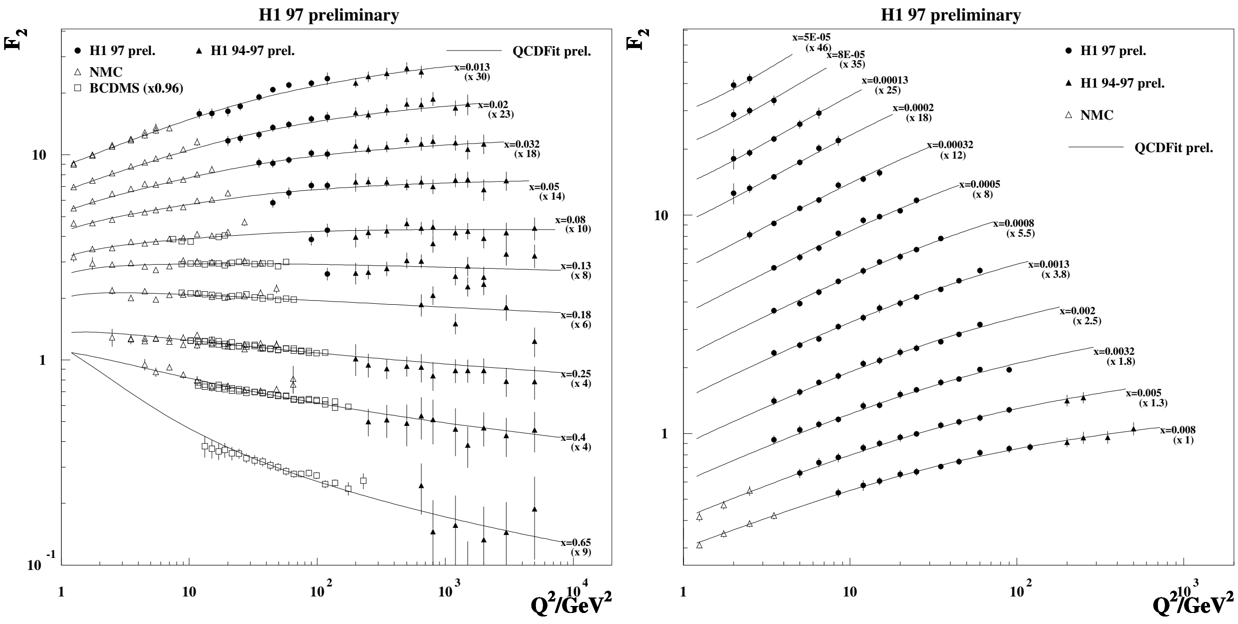

Figure 3: Structure function measurements by H1 (solid circles and triangles), NMC (open triangles) and BCDMS (open squares) as a function of Q^2 in bins of x. The left hand figure shows the high x region with approximate scaling in the region $x \approx 0.1$, the right hand figure the low x region with strong scaling violations. The two H1 data sets correspond to the high and low Q^2 region as defined in section 3. Also shown is a NLO QCD fit based on the data (solid line).

Silicon Tracker (BST) has been used for tracking and background rejection. In 1997, H1 recorded an integrated luminosity of 15 pb^{-1} in the range 10 GeV^2 $< Q^2 \leq$ 120 GeV^2, and of 2 pb^{-1} in the range 2 GeV^2 $\leq Q^2 <$ 10 GeV^2 in a dedicated run with specific trigger settings [3]. In the high Q^2 region with $Q^2 \geq$ 200 GeV^2, the H1 analysis uses an integrated luminosity of 37.0 pb^{-1} collected from 1994 to 1997 [10].

The kinematic variables y (or x) and Q^2 can be determined from the electron, the hadronic final state, or a combination of both. This leads to an overconstrained determination of the kinematics and allows cross checks as well as the choice of the method with the best experimental precision for a given kinematic region. Using the electron information alone, the event kinematics can be reconstructed with the electron method where

$$Q_e^2 = 4E_e{E_e}'\cos^2\frac{\theta_e}{2} \quad \text{and} \quad y_e = 1 - \frac{{E_e}'}{E_e}\sin^2\frac{\theta_e}{2}\ . \tag{4}$$

Here ${E_e}'$ and θ_e are the energy and polar angle, respectively, of the scattered electron. For both the H1 and the ZEUS detector, reference frames are used where the unscattered electron beam has a polar angle of $\theta = 180°$. Another commonly used method is the double angle method [11], in which the polar angle of the hadronic jet and of the electron are combined to reconstruct the event kinematics. This method is independent of the energy scale and therefore is not sensitive to potential calorimeter miscalibrations.

The cross section is determined by converting the number of events counted in bins of x and Q^2, after background subtraction and using Monte Carlo acceptance calculations, into a bin averaged cross section. In the low Q^2 region, main contributions to the systematic error of the cross section measurement result from the energy calibration (systematic studies require large statistics, e.g. cell-by-cell calibration and local effects) and photoproduction background. With the 1997 luminosity, systematic errors of 3–5% and statistical errors of 1–2% for the measurement of F_2 at low Q^2 could be achieved.

In figure 1, the preliminary measurement of the reduced cross section with the 1997 H1 data is shown. A smooth transition to the fixed target data at large x and a steep rise of F_2 towards low x can be observed. The data and a NLO QCD fit to the H1, NMC, and BCDMS experimental data as described in section 2 show very good agreement. The departure of the reduced cross section from the behavior of F_2 for high y can be attributed to the contribution of F_L.

The structure function F_2 in the range 35 GeV$^2 \leq Q^2 \leq$ 650 GeV^2 as measured by ZEUS is shown in figure 2. Since the electromagnetic part of the double differential DIS cross section is proportional to $1/Q^4$, the statistics decreases rapidly with increasing Q^2. The overall precision of the measurement has clearly improved as a result of the increased statistics of the 1997 HERA operation.

In figure 3, the experimental data from the H1, BCDMS, and NMC experiments is compared with the cross sections obtained from the QCD fit as a function of Q^2 in fixed bins of x. In the left part of figure 3, one sees the region of approximate Bjorken scaling, while the right part shows the scaling violations in the low x region. The fit constitutes a very good quantitative description of the experimental data.

4 Determination of F$_L$

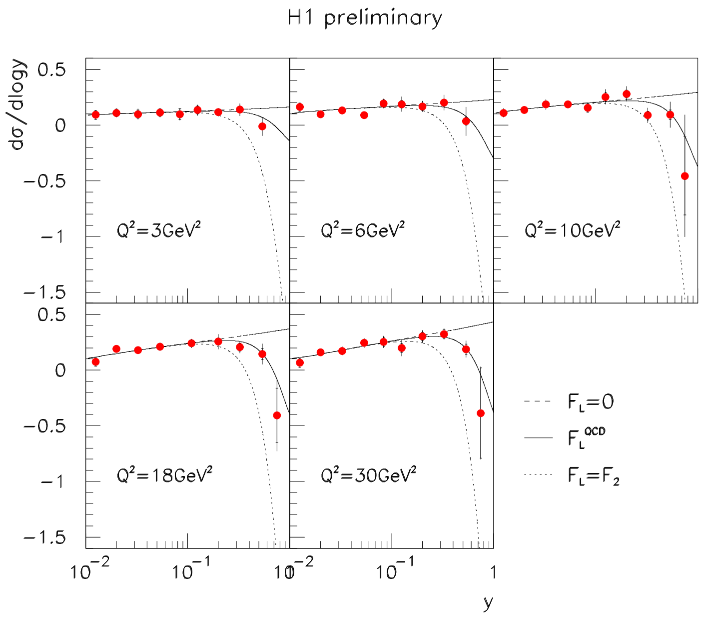

Figure 4: Measurement of the derivative $\partial\sigma_r/\partial \log y$. The curves represent the QCD cross section fit result (solid curve), and the fit result with the replacements $F_L = 0$ (dashed curve, essentially a straight line) and $F_L = F_2$ (dotted curve).

The determination of F_L is possible only at high values of y where the term involving F_L in equation (1) becomes sizeable with respect to F_2. In order to determine F_L under the current HERA conditions of fixed beam energies, the H1 collaboration has employed two methods [14], [3]. First, the conventional "subtraction" method, where the value of F_2 extrapolated with a DGLAP evolution equation is subtracted from the measured reduced cross section to obtain $F_L = Y_+/y^2(F_2 - \sigma_r)$. Second the new "derivative" method: Defining the derivative $\partial\sigma_r/\partial \log y$ as

$$\frac{\partial \sigma_r}{\partial \log y} = \frac{\partial F_2}{\partial \log y} - F_L \cdot 2y^2 \cdot \frac{2-y}{Y_+^2} - \frac{\partial F_L}{\partial \log y} \cdot \frac{y^2}{Y_+} \tag{5}$$

one can determine F_L with increased sensitivity with respect to the F_2 part. The data were binned in y and for adjacent bins, differences $\Delta\sigma_r$ were calculated from the corresponding reduced cross sections. Using Monte Carlo calculations, a bin center correction was applied to transform the ratio $\Delta\sigma_r/\Delta \log y$ to a value which represents the evaluation of the derivative $\partial\sigma_r/\partial \log y$ at the mean of the two adjacent

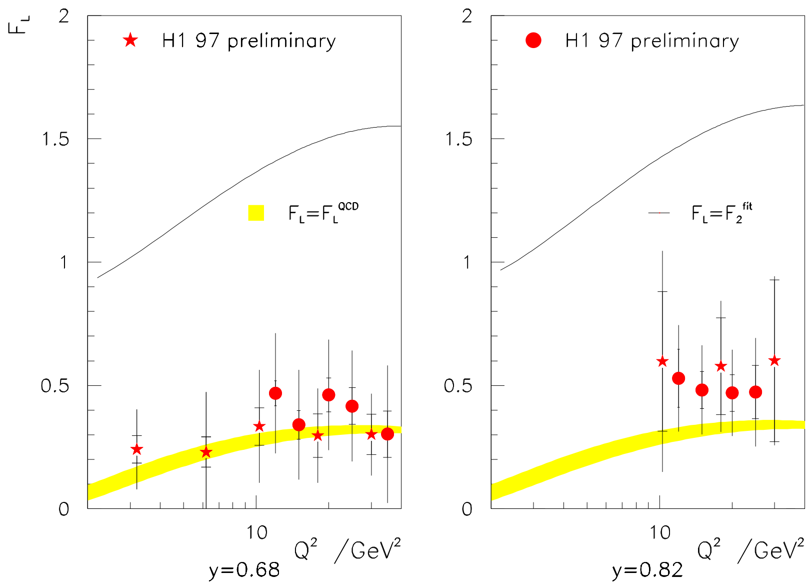

Figure 5: Determination of F_L using the subtraction method (full circles) and the derivative method (stars) for two different values of y. The narrow band represents the uncertainty range of F_L when calculated using the gluon and quark distributions determined with the NLO QCD fit to the H1, NMC and BCDMS data. The solid line represents the QCD cross section fit result with the replacement $F_L = F_2$. In all figures, the inner error bars represent the statistical errors and the total error bars represent the statistical and systematic errors in quadrature.

y points entering the calculation. The result of this operation is shown in figure 4. The figure also shows the results of the NLO QCD fit from figure 1 using different assumptions on F_L. When using the result for F_2 obtained from the QCD fit with the replacement $F_L = 0$, the extrapolation of $\partial\sigma_r/\partial \log y$ into the high y region basically follows a straight line. Consequently, a parametrization of the form $\partial F_2/\partial \log y = A \log y + B$ has been assumed and the values A and B were obtained from fits in the region $y < 0.2$ for each value of Q^2. F_L was then derived according to equation (5) at the individual y values[4], where the difference between the assumption of linearity and the QCD fit expectation for the quantity $\partial F_2/\partial \log y$ enters into the error of the determination of F_L.

The results of both the subtraction method and the derivative method are shown in figure 5. The two methods are consistent among each other and with F_L as calculated from a NLO QCD fit to F_2. With the derivative method, lower values of Q^2 can be reached since the assumption on F_2 is not based on QCD. Furthermore, the experimental error for the derivative method is smaller since the part of the systematic error on the reduced cross section which is common for all values of y cancels when forming the differences $\Delta\sigma_r$.

5 The Very Low Q^2 Region

The interest in the transition between the kinematic region of DIS with its theoretical description through perturbative QCD and photoproduction described by Regge phenomenology has lead both H1 and ZEUS to extend the measurement of the proton substructure to the lowest possible Q^2 region. In order to reach values as low as $Q^2 = 0.35$ GeV^2 with the existing instrumentation of the H1 and ZEUS detectors, HERA was operating with the interaction point shifted by 70 cm into the forward direction during a part of

[4]The term containing $\partial F_L/\partial \log y$ in equation (5) can be shown to be negligible.

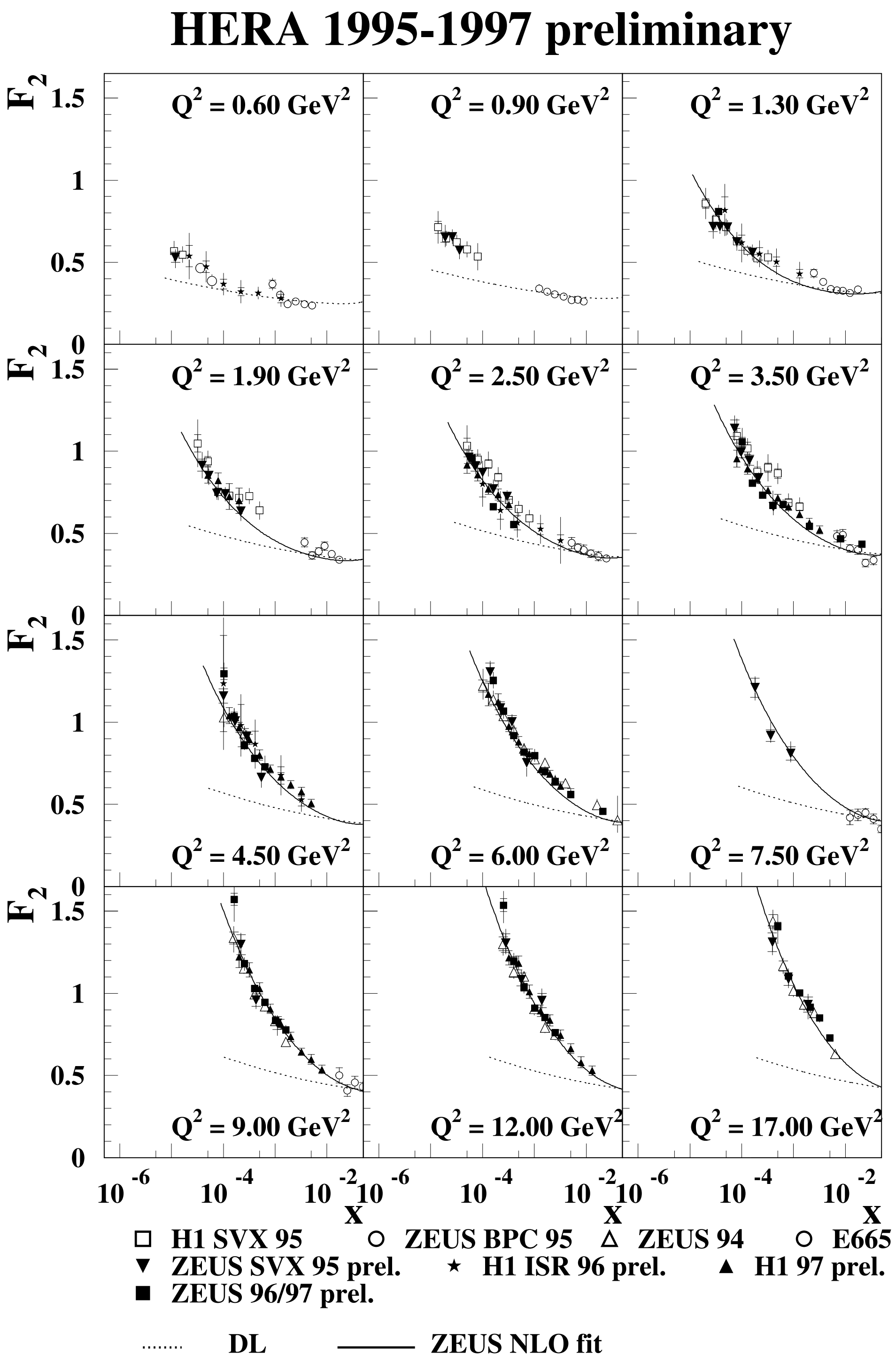

Figure 6: The structure function F_2 in the very low Q^2 region as measured by H1 and ZEUS using the different methods described in the text. Also shown are fits to the data using the Regge based model by Donnachie and Landshoff (DL, dotted line) and a NLO QCD fit (solid line).

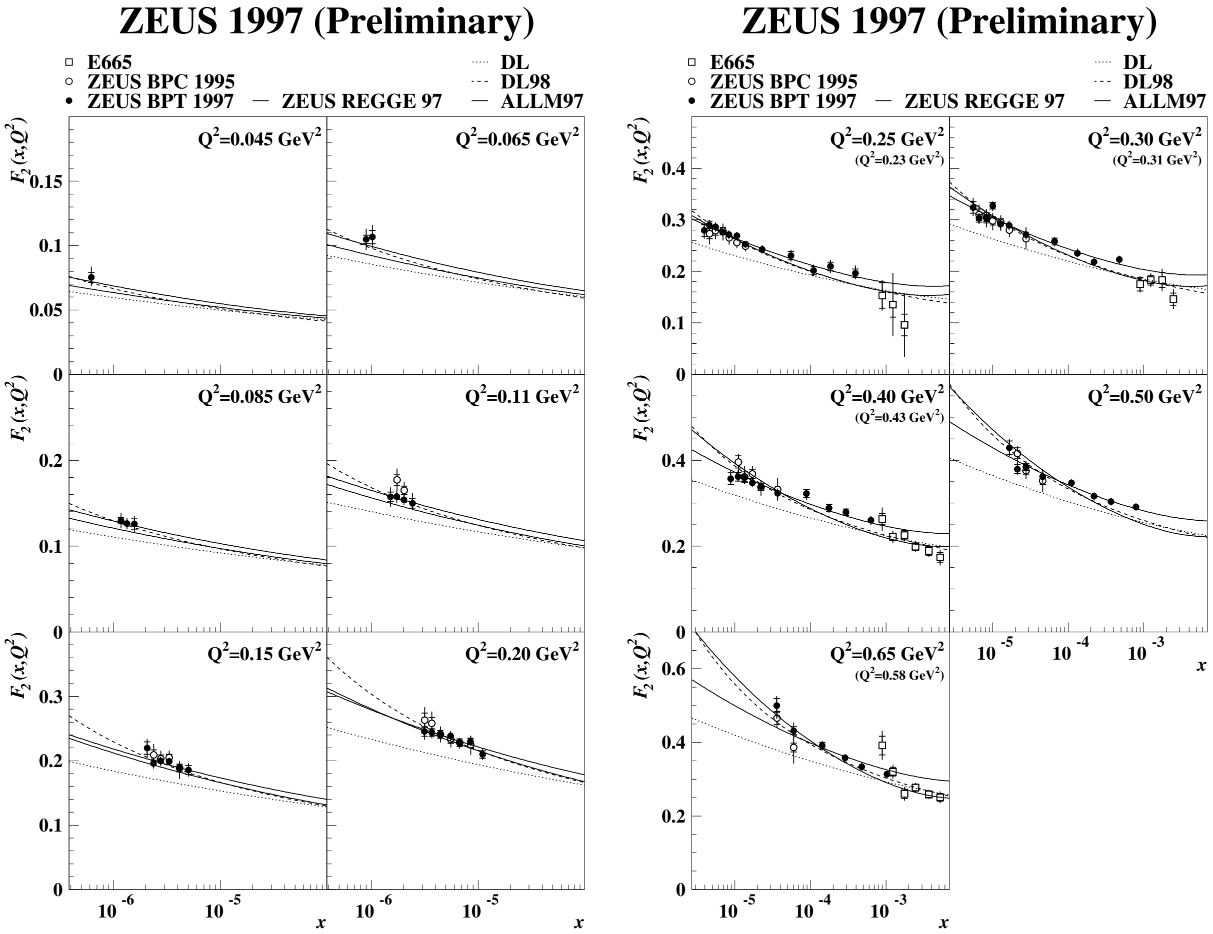

Figure 7: The structure function F_2 as a function of x in bins of Q^2 ranging from 0.045 GeV^2 to 0.65 GeV^2, as measured by the ZEUS collaboration with the Beam Pipe Calorimeter (BPC) and the Beam Pipe Tracker (BPT). The Q^2 values in paranthesis in the right hand figure correspond to the E665 measurements. The four different fits which are shown are described in the text. The ZEUS REGGE97 parametrization is the solid lines which at high values of x always predicts higher values of F_2 when compared to the other solid line that describes the ALLM97 fit.

1995 [12], [4]. H1 has also used radiative events to investigate the kinematic region down to $Q^2 \approx 0.2$ GeV^2 [3]. With this method, the cross section of highly radiative events $\sigma(ep \rightarrow e\gamma X)$ is measured, where the photon is detected by a tagger in the HERA tunnel, about 100 m upstream from the H1 detector in the electron direction.

Finally, the HERA experiments have instrumented the region very close to the beam pipe in the backward direction. ZEUS has installed the Beam Pipe Calorimeter (BPC) in 1995, which was supplemented by the Beam Pipe Tracker (BPT) in 1997. The analysis with these new detector components will be discussed in detail below. H1 has started to operate its Very Low Q^2 (VLQ) detector, consisting of a calorimetric and tracking part, in 1998.

In figure 6, the different measurements of F_2 at very low Q^2 performed by the H1 and ZEUS collaborations are compared. The agreement among them can be seen to be very good. Shown in the figure are also two different fits to the data. The first fit uses the "conventional" Regge based model by Donnachie and Landshoff (DL), assuming a Reggeon and one "soft" Pomeron trajectory whose intercept of about 1.08 is derived from soft hadronic interactions [13]. This DL-fit describes the data only in the lowest Q^2 bin with an acceptable precision and shows an increasing disagreement with the data for increasing values of Q^2. Second, a NLO QCD fit to the ZEUS data as described in section 2 shows very good agreement

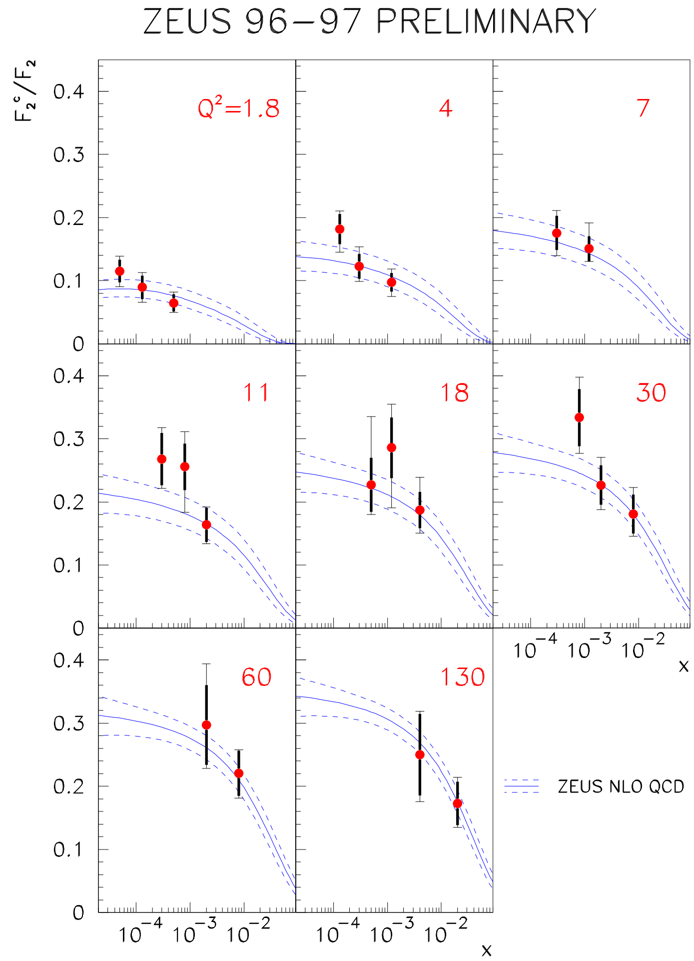

Figure 8: $\sigma_{tot}^{\gamma^* p}$ versus Q^2 for different values of the center of mass energy W. Shown are the new measurements with the ZEUS BPT (full circles) and previous measurements of H1 and ZEUS for DIS (open squares) and interactions of quasi-real photons with protons (full triangles). The four fits which are shown are described in the text.

in its range of application for $Q^2 > 1$ GeV^2.

Recently, the ZEUS collaboration has presented new preliminary results for the kinematic range 0.045 GeV^2 $< Q^2 <$0.65 GeV^2 using both the BPC and the BPT [15]. These results are based on the analysis of an integrated luminosity of about 3.9 pb^{-1} which was recorded with special trigger settings during six dedicated weeks in 1997. Cross sections were calculated in bins of Q^2 and y and $F_2(x, Q^2)$ was extracted using an iterative bin-to-bin unfolding method.

The F_2 values measured with this analysis are shown in figure 7 as a function of x in bins of fixed Q^2. Where applicable, the results from E665 [16] and from the analysis using the BPC only as shown in figure 6 have been included.

To study the transition region from photoproduction to DIS more closely it is convenient to present the low Q^2 data in terms of the interaction of the virtual photon with the proton. At small x, the total $\gamma^* p$ cross section is related to F_2 according to

$$\sigma_{tot}^{\gamma^* p}(W, Q^2) \approx \frac{4\pi^2\alpha}{Q^2} F_2(x, Q^2) \ , \tag{6}$$

where for small values of x, the center of mass energy of the $\gamma^* p$ system can be approximated by $W \approx Q^2/x$. In figure 8, $\sigma_{tot}^{\gamma^* p}$ is plotted as a function of Q^2 for different values of W. The new data from the BPT can be seen to fill a kinematic region in which previously no measurements were available, linking the measurements of γp interactions with those obtained from DIS at HERA. Four different fits are shown in figures 7 and 8. Two of the fits are global distributions from Donnachie and Landshoff: the "conventional" fit described above (DL), and a fit which uses an additional "hard" pomeron which becomes increasingly dominant for higher Q^2 values [17]. The ALLM97 parametrization [18], [19] uses a Regge-style approach with a QCD-inspired *ansatz* for the extension into the high Q^2 region. Finally, the ZEUS REGGE97 parametrization is similar to the one used in the global DL fit, where the ZEUS fit was performed on the data from earlier γp experiments at low W and the BPT $\gamma^* p$ data [15], [4].

6 The Charm Contribution F_2^c to F_2

The dominant process of $c\bar{c}$ production in DIS is boson gluon fusion in which a photon coupling to the incoming electron interacts with a gluon in the proton to form a $c\bar{c}$ pair [6]. The relation between the cross section of charm production in DIS (σ^c) and F_2^c is given by substituting σ and F_2 in equation (1) by the corresponding expressions. The contribution of the F_L^c term is expected to be on the order of $1 \sim 2\%$ in the kinematic region explored by the analysis described below and therefore has been neglected.

Originally, σ^c has been measured by both H1 and ZEUS through the decay of the $c \to D^{*\pm}$ along the chain $D^{*\pm} \to D^0\pi^\pm \to (K^\mp\pi^\pm)\pi^\pm$ [20], [21]. The most recent measurement of F_2^c at HERA was presented by ZEUS using the decays $D^0 \to K^\mp\pi^\pm$ and $D^0 \to K^\mp 2\pi^\pm\pi^\mp$ [22]. For this analysis, an integrated luminosity of 37 pb^{-1}, collected during 1996 and 1997, was used. The $D^{*\pm}$ is tagged using the tight kinematic constraints of the decay chain. The $D^{*\pm}$ production cross section is first measured in a restricted region of the transverse momentum $p_T(D^*)$ and the rapidity $\eta(D^*)$ of the D^* in bins of Q^2 and x or y. The extrapolation of F_2^c is then obtained by scaling the measured cross section in a given bin by the ratio of the theoretically expected F_2^c and the cross section in the bin as predicted from Monte Carlo. This method accounts for acceptance corrections, the hadronization fraction of charm to $D^{*\pm}$ and the branching ratio for the decays $D^{*\pm} \to (K^\mp\pi^\pm)\pi^\pm$ and $D^{*\pm} \to (K^\mp 2\pi^\pm\pi^\mp)\pi^\pm$.

In the left part of figure 9 the results for F_2^c from ZEUS are shown as a function of x for fixed values of Q^2. One can observe the same qualitative behavior for F_2^c as for F_2 (compare figure 1), namely a steep rise with decreasing x due to the gluon contribution. In the right part of figure 9, F_2^c is expressed as a fraction of F_2. One obtains a sizeable, but not constant contribution of F_2^c to the proton structure function of the order $0.1 \lesssim F_2^c/F_2 \lesssim 0.3$ in the kinematic range accessible at HERA. In figure 10, F_2^c is shown as a function of Q^2 for constant x. Qualitatively, the same scaling violating behavior as for F_2 can be observed (compare figure 3).

Shown in all figures are the expected values of F_2^c which were calculated using the gluon distribution derived from the NLO QCD fit the ZEUS collaboration has performed on its inclusive DIS cross section measurements [4]. The agreement between the fits and the data can be seen to be very good in all figures.

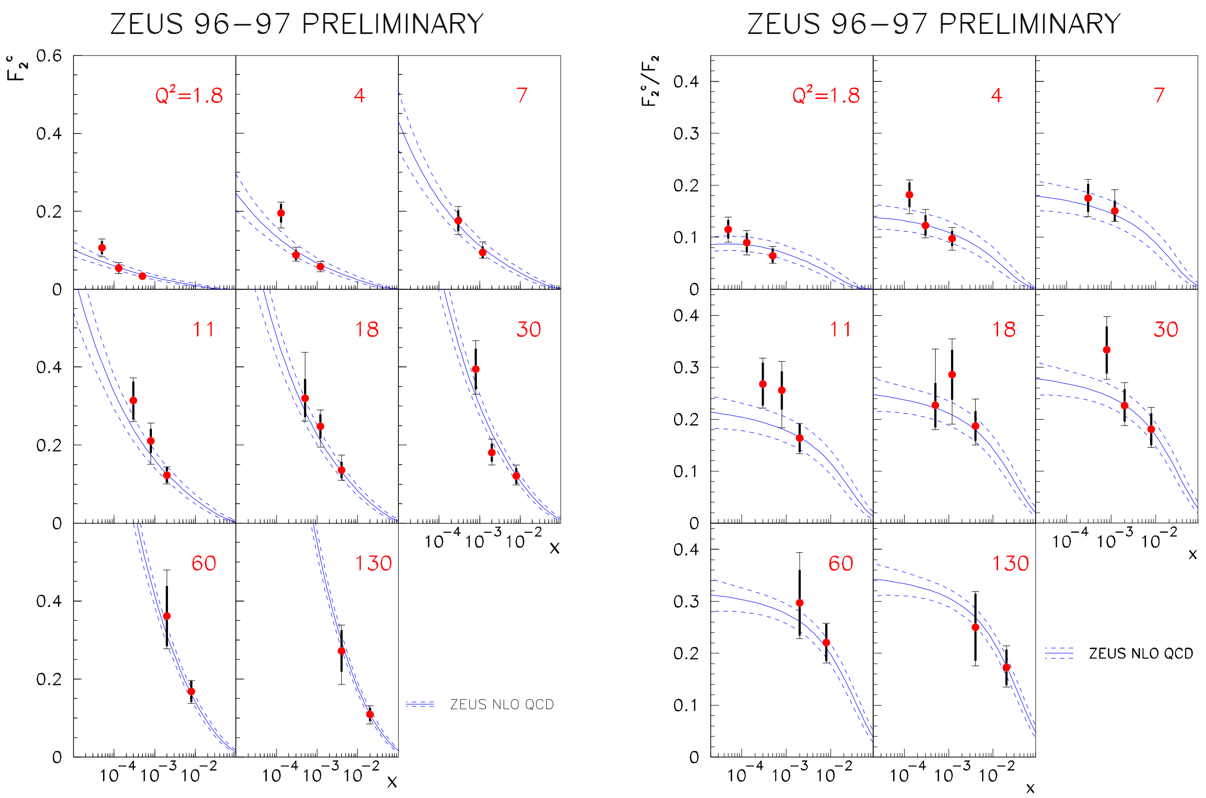

Figure 9: The charm contribution F_2^c to the proton structure function F_2 (left) and the ratio F_2^c/F_2 (right) as a function of x in fixed bins of Q^2. The inner error bars show the statistical errors and the outer ones the statistical and systematic errors in quadrature. The values of F_2^c as predicted from the ZEUS NLO QCD fit (solid curve) with their errors (dashed curve) are also shown.

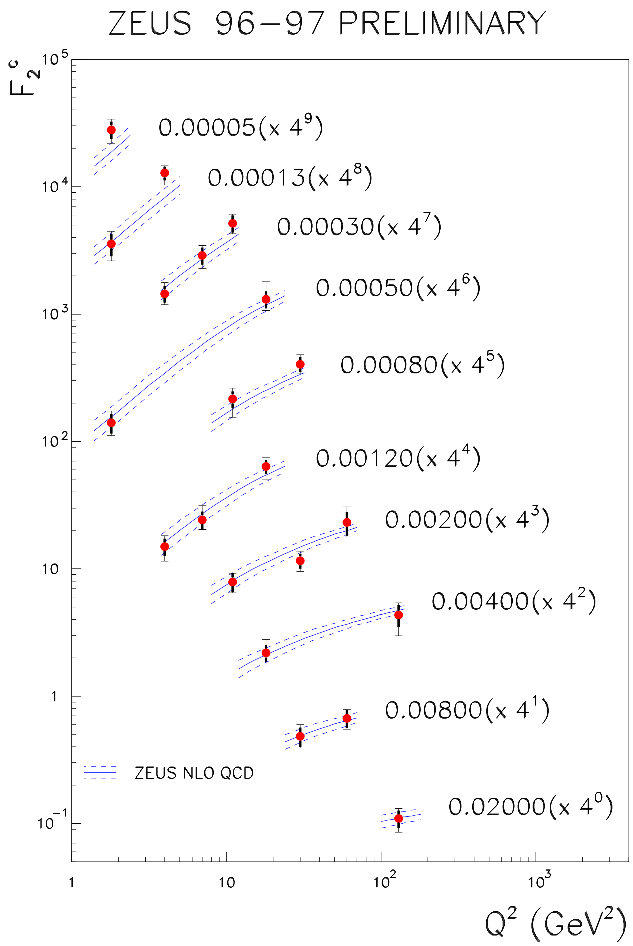

Figure 10: The charm contribution F_2^c to the proton structure function F_2 as a function of Q^2 for fixed values of x. The inner error bars show the statistical errors and the outer ones the statistical and systematic errors in quadrature. The values of F_2^c as predicted from the ZEUS NLO QCD fit (solid curve) with their errors (dashed curve) are also shown.

7 The Gluon

7.1 The Gluon Distribution from Scaling Violations

The most precise way to determine the gluon distribution $x \cdot g(x)$ is from the scaling violations of F_2 which are due to gluon *bremsstrahlung* from quarks and quark pair production from gluons. The parametrization of the gluon distribution is contained in the NLO QCD fits to F_2 described in section 2. In figure 11, the gluon distribution xg and the singlet distribution $x\Sigma$, as they were determined from a NLO QCD fit performed by the ZEUS collaboration [4], [23] are shown. The error bands include the experimental systematic errors, the statistical error of the data, and the uncertainties from the values of $\alpha_s(M_Z^2)$, the strange quark contents of the proton and the charm mass. In addition, errors of the fit procedure are included which originate from possible biases due to the choice of errors entering the χ^2 (statistical errors alone versus statistical and systematic errors added in quadrature), the choice of the starting point Q_0^2 of the evolution and the choice of the gluon distribution parametrization. The gluon distribution can

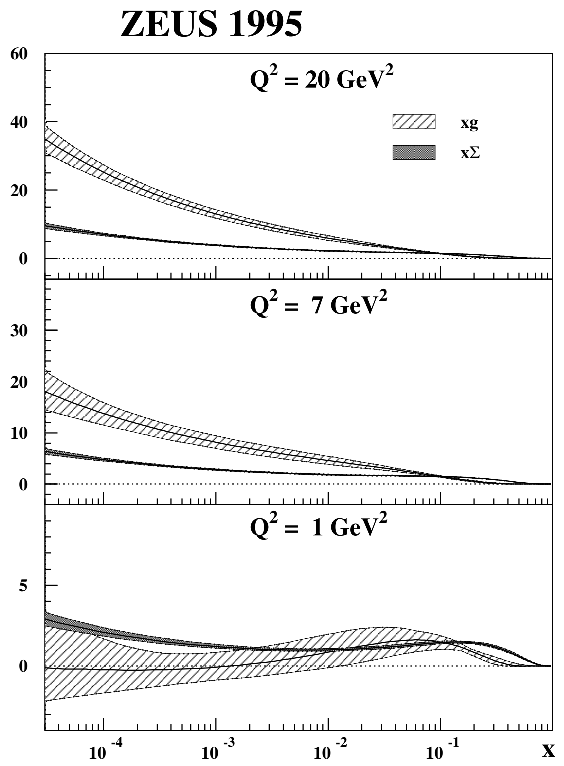

Figure 11: The quark singlet momentum distribution $x\Sigma$ (shaded) and the gluon momentum distribution xg (hatched) as a function of x at fixed values of Q^2 from the ZEUS NLO QCD fit. The error bands correspond to the quadratic sum of all error sources.

be seen to evolve much faster than the sea distribution, which dominates the distribution $x\Sigma$ at small values of x. At $Q^2 \gg 1$ GeV^2, the gluon "drives" the sea and is therefore responsible for the fast rise of F_2 with decreasing x. At $Q^2 \approx 1$ GeV^2, the gluon behaves valence-like. The distribution xg becoming negative at small values of x for backwards evolved values of Q^2 is not necessarily in contradiction with perturbative NLO QCD as long as the physical quantities derived from that distribution (cross sections and structure functions) are positive. Notably, the analysis applies the DGLAP QCD formalism in the transition region to photoproduction without observing a breakdown of that formalism.

7.2 The Gluon Distribution from Charm Production

H1 has determined the gluon distribution from charm production in DIS ($Q^2 > 2$ GeV) and photoproduction ($Q^2 \approx 0$ GeV) [20] within the framework of the NLO QCD programs HVQDIS [24] and FMNR [25], respectively. In leading order of the process $\gamma g \to c\bar{c}$, the momentum fraction in the infinite momentum frame is given by $x_g = (M^2 + Q^2)/ys$, where M is the invariant mass of the $c\bar{c}$ system. The *observed* gluon distribution x_g^{OBS} is different from x_g due to the presence of gluon radiation and the experimental conditions, under which not charm quarks but D^* mesons are measured.

The measurement of the gluon distribution proceeds in two main steps: First, the visible D^* cross section is measured as a function of x_g^{OBS}. Second, the gluon distribution at the "true" x_g is extracted from the observed cross section and the observed gluon density by means of an unfolding integral after subtraction of the quark-induced contribution to the visible cross section.

The resulting gluon distributions at an average scale $\mu^2 = 25$ GeV^2 are shown in figure 12. One can observe a good agreement between the gluon distributions extracted from the photoproduction and DIS D^* analysis. The agreement with the gluon distribution obtained by H1 from the F_2 scaling violations [26] is also good.

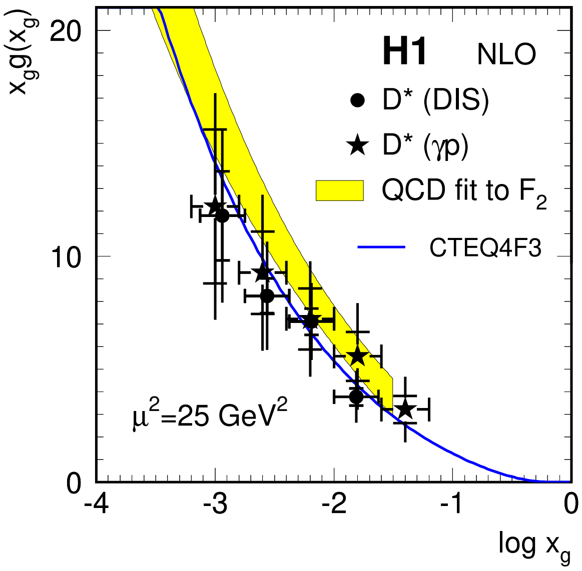

Figure 12: Comparison of the gluon distributions obtained from the D^* analysis with the H1 results from scaling violations and the CTEQ4F3 [27] parametrization. The systematic error is the quadratic sum of all contributions, dominated by the uncertainties of the charm quark mass and the fragmentation parameter. The inner error bars represent the statistical errors.

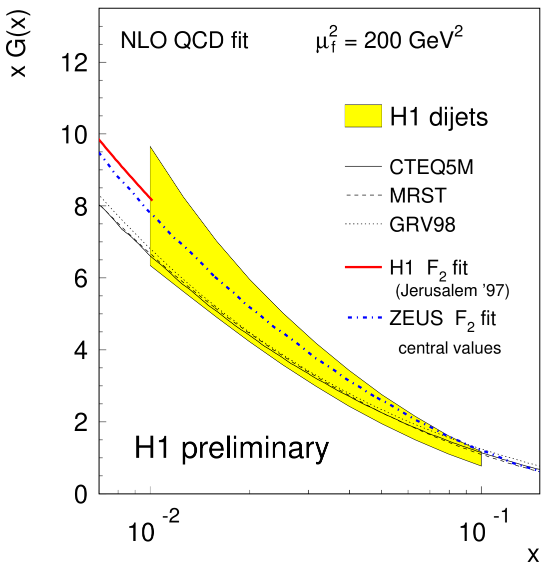

Figure 13: The gluon distribution in the proton from a NLO QCD fit to dijet cross sections. The error band includes experimental and theoretical uncertainties as well as the uncertainty on $\alpha_s(M_Z^2)$. It is compared to the gluon distributions obtained in different global analyses and to the central values of the H1 and ZEUS gluon distribution from scaling violations.

7.3 The Gluon Distribution from Dijet Cross Sections

Dijet production is sensitive to the gluon distribution through the formation of quark–antiquark pairs by the process of boson gluon fusion described above. In a recent analysis [28] the gluon distribution was derived from a NLO QCD fit to the DIS dijet cross sections. Using a value of $\alpha_s(M_Z^2) = 0.119 \pm 0.005$, the fit was performed in the region 200 GeV$^2 < Q^2 <$5000 GeV^2. Simultaneously included in the procedure was a fit to the inclusive neutral current DIS ep-cross sections (compare section 3) to constrain the quark distribution in the proton. Jets were defined by the inclusive $k_\perp$ algorithm [29] In the leading order picture, the gluon distribution is probed at the fractional proton momentum ξ which is equivalent to the variable x_g from the previous subsection with M replaced by the invariant mass of the dijet system. The analysis was performed at a factorization scale $\mu_f^2 = 200$ GeV^2 in the range $0.01 < \xi < 0.1$; The preliminary result of the analysis is shown in figure 13.

8 Summary

The H1 and ZEUS Experiments at HERA have measured the proton structure functions F_2 in a kinematic range spanning more than 5 orders of magnitude in both Q^2 and x. For $Q^2 \lesssim 100$ GeV^2, F_2 has been measured with a systematics dominated error of $\lesssim 5\%$. The F_2 data is well described by NLO QCD fits and at high values of y, effects on the reduced cross section due to F_L become visible. The deviation of the reduced cross section from the expected value of F_2 has been used to determine F_L. The results show good agreement with calculations of F_L using a NLO QCD fit to F_2.

In the transition region from DIS to photoproduction, new measurements were presented using newly installed detector components of the ZEUS detector which extend the measurement of F_2 into previously unprobed regions with Q^2 as low as 0.045 GeV^2. In the region $Q^2 \geq 0.6$ GeV^2, measurements by H1 and ZEUS using different methods show good agreement. The data were compared to the predictions from different fits: The Regge based global fit by Donnachie and Landshoff needs an additional "hard" Pomeron in order to give a reasonable description of the data for all values of Q^2 while for a similar fit performed to the ZEUS data and to results from γp experiments at low W, the assumption of one Reggeon and one "soft" Pomeron is sufficient. For Q^2 values as low as 1 GeV^2, the data are consistently described by a NLO QCD fit.

For the charm contribution F_2^c to F_2, results with increased statistics are available which are in good agreement with NLO QCD. F_2^c shows the same qualitative behavior as F_2, i.e. a steep rise with decreasing x at constant Q^2 and scaling violations when plotted as a function of Q^2 for constant x. The contribution of F_2^c to the proton structure function is of the order $0.1 \lesssim F_2^c/F_2 \lesssim 0.3$ in the kinematic range accessible at HERA.

The gluon distribution in the proton has been measured using different independent methods. The most precise measurements are from the F_2 scaling violations. Comparisons of the gluon distribution and the sea distribution show a steeper rise with decreasing x for the gluon distribution. This rise of the gluon distribution towards small values of x becomes steeper for increasing values of Q^2, while one obtains a valence-like behavior at $Q^2 = 1$ GeV^2. Measurements of the gluon distribution have also been obtained from the analysis of charm and dijet events. These measurements yield results in a region with larger values of x and show good agreement with the results from the scaling violations in the region of overlap.

References

[1] A. van Sighem, these proceedings.

[2] Yu.L. Dokshitzer, *Sov. Phys. JETP* **46**, 641 (1977);
V.N. Gribov and L.N. Lipatov, *Sov. J. Nucl. Phys.* **15**, 438 and 675 (1972); G. Altarelli and G. Parisi, *Nucl. Phys.* B **126**, 298 (1977).

[3] M. Klein, proceedings of the 29th International Conference on High Energy Physics (ICHEP 98), Vancouver, July 1998.

[4] ZEUS Collab., *Eur. Phys. J.* **C 7**, 609 (1999)

[5] A.D. Martin, R.G. Roberts, W.J. Stirling, *Phys. Lett.* B **387**, 419 (1996).

[6] E. Laenen *et al.*, *Nucl. Phys.* B **392**, 162 (1993);
S. Riemersma *et al.*, *Phys. Lett.* B **347**, 143 (1995).

[7] NMC Collab., M.Arneodo *et al.*, *Nucl. Phys.* B **483**, 3 (1997).

[8] BCDMS Collab., A.C. Benvenuti *et al.*, *Phys. Lett.* B **223**, 485 (1989).

[9] A. Quadt, proceedings of the 29th International Conference on High Energy Physics (ICHEP 98), Vancouver, July 1998.

[10] M. Fleischer, proceedings of the 29th International Conference on High Energy Physics (ICHEP 98), Vancouver, July 1998.

[11] S.Bentvelsen, J.Engelen, P. Kooijman in: Physics at HERA, vol.1, 23 (1991); K.C. Hoeger, in: Physics at HERA, vol.1, 43 (1991).

[12] H1 Collab., C. Adloff *et al.*, *Nucl. Phys.* B **497**, 3 (1997).

[13] A. Donnachie and P.V. Landshoff, *Z. Phys.* C **61**, 139 (1994).

[14] H1 Collab., S. Aid *et al.*, *Phys. Lett.* B **393**, 452 (1997).

[15] Ch. Amelung, proceedings of the 7th International Workshop on Deep Inelastic Scattering and QCD (DIS 99), Zeuthen, April 1999.

[16] E665 Collab., M.R. Adams *et al.*, *Phys. Rev.* D **54**, 3006 (1996).

[17] A. Donnachie and P.V. Landshoff, hep-ph/9806344 v02.

[18] H. Abramowicz, *et al.*, *Phys. Lett.* B **269**, 465 (1991).

[19] H. Abramowicz, A. Levy, DESY 97-251.

[20] H1 Collab., C. Adloff *et al.*, *Nucl. Phys.* B **545**, 21 (1999).

[21] W. Verkerke, proceedings of the 29th International Conference on High Energy Physics (ICHEP 98), Vancouver, July 1998.

[22] I. Redondo, proceedings of the 7th International Workshop on Deep Inelastic Scattering and QCD (DIS 99), Zeuthen, April 1999.

[23] M. Botje, proceedings of the 7th International Workshop on Deep Inelastic Scattering and QCD (DIS 99), Zeuthen, April 1999.

[24] B.W. Harris and J. Smith, preprint DESY 97-111, FSU-HEP-970527, May 1997.

[25] S. Frixione *et al.*, *Phys. Lett.* B **348**, 633 (1995); *Nucl. Phys.* B **454**, 3 (1995).

[26] H1 Collab., contributed paper to International Europhysics Conference on High Energy Physics (EPS HEP 97), paper 260, Jerusalem, August 1997; V. Chekelian, proceedings of the 18th International Symposium on Lepton-Photon Interactions (LP'97), Hamburg, July 1997.

[27] H.L. Lai *et al.*, *Phys. Rev.* D **55**, 1280 (1997).

[28] M. Wobisch, proceedings of the 7th International Workshop on Deep Inelastic Scattering and QCD (DIS 99), Zeuthen, April 1999.

[29] S.D. Ellis and D.E. Soper, *Phys. Rev.* D **48**, 3160 (1993).